

# Mineralogical characterization of scalings formed in geothermal sites in the Upper Rhine Graben before and after the application of sulfate inhibitors

Ruth Haas-Nüesch<sup>a,b</sup>, Frank Heberling<sup>a,\*</sup>, Dieter Schild<sup>a</sup>, Jörg Rothe<sup>a</sup>, Kathy Dardenne<sup>a</sup>, Sabine Jähnichen<sup>c</sup>, Elisabeth Eiche<sup>b</sup>, Christian Marquardt<sup>a</sup>, Volker Metz<sup>a</sup>, Thorsten Schäfer<sup>a,d</sup>

<sup>a</sup> Karlsruhe Institute of Technology, Institute for Nuclear Waste Disposal (KIT-INE), Hermann-von-Helmholtz Platz 1, 76344, Eggenstein-Leopoldshafen, Germany

<sup>b</sup> Karlsruhe Institute of Technology, Institute of Applied Geosciences, Adenauer Ring 20b, 76131, Karlsruhe, Germany

<sup>c</sup> VKTA – Strahlenschutz, Analytik & Entsorgung Rossendorf e. V. Postfach 510119, 01314, Dresden, Germany

<sup>d</sup> Friedrich-Schiller-Universität Jena, Institut für Geowissenschaften, Burgweg 11, 07749, Jena, Germany

## ARTICLE INFO

### Keywords:

Geothermal scaling  
Sulfate inhibitor  
Galena  
Elemental lead  
Arsenic  
Antimony

## ABSTRACT

Scale formation processes in the surface installations of geothermal power plants may have a negative effect on power plant performance. In addition, scales formed within the geothermal water circuit frequently accumulate natural radionuclides. Consequently, scale formation may lead to radiation dose rates, which are of radiological concern, and deposits, which may have to be disposed as radioactive waste. In order to minimize these problems and to foster geothermal power plant availability, it is of major interest to understand scale formation processes and to develop methods for their inhibition. One important pre-requisite towards this goal is a sound mineralogical and geochemical characterization of the formed material.

Geothermal brines at sites in the Upper Rhine Graben are in general highly mineralized and become, upon cooling in the heat exchanger, supersaturated with respect to sulfate solid-solutions, e.g. (Ba,Sr)SO<sub>4</sub>, and other mineral phases. Some geothermal power plants very successfully tested the application of sulfate scaling inhibitors. Here we present mineralogical analyses of scale samples from geothermal power plants in the Upper Rhine Valley deposited in absence and presence of sulfate scaling inhibitors. Solid samples are investigated using wet-chemistry (after digestion), XRPD, SEM-EDX, XPS, EA-IRMS, Raman spectroscopy, and XANES (for explanation of abbreviations, see main text).

Samples of scales deposited in the absence of a sulfate scaling inhibitor mainly consist of two phases. The largest part is made up of a barite type (Ba,Sr,Ca)SO<sub>4</sub> solid-solution. Traces of Ra occurring in the scaling are assumed to be incorporated in the barite type solid solution. Further minor phases are sulfide phases, either an X-ray amorphous nano-particulate phase or galena (PbS).

Since the application of the sulfate inhibitor, sulfate minerals are no longer detectable in the scale samples. Subsequent scalings are Pb-dominated and consist mainly of galena (PbS), elemental lead (Pb), arsenic (As) and antimony (Sb). As and Sb are likely present as a nanocrystalline intermetallic mixed compound ((Sb, As) or Pb<sub>3</sub>(Sb,As)<sub>2</sub>S<sub>3</sub>). The absence of barite-type minerals demonstrates the success of the application of the sulfate inhibitor. The precipitation of elemental Pb, As, and Sb, which are more noble than iron, may enhance the corrosion of mild steel pipes in the geothermal water circuit. Elution tests and oxidation of the scalings upon storage at atmospheric conditions demonstrate that proper disposal of the toxic heavy metal and metalloid containing scalings may be challenging.

## 1. Introduction

The western part of the Upper Rhine Graben (SW Germany, NE France) is a tertiary rift system showing a geothermal anomaly with a high temperature gradient and temperatures up to 130 °C at 1500 m

depth (Dezayes et al., 2015). In the last decades, several geothermal projects started to access the deeper part of the reservoir. The encountered geothermal brines are highly mineralized (Sanjuan et al., 2016). Decreasing pressure and temperature at the production well and in the heat exchanger leads to mineral precipitation in the surface and

\* Corresponding author.

E-mail addresses: ruth.haas@kit.edu (R. Haas-Nüesch), frank.heberling@kit.edu (F. Heberling), dieter.schild@kit.edu (D. Schild), joerg.rothe@kit.edu (J. Rothe), kathy.dardenne@kit.edu (K. Dardenne), sabine.jaehnichen@vkta.de (S. Jähnichen), elisabeth.eiche@kit.edu (E. Eiche), christian.marquardt@kit.edu (C. Marquardt), volker.metz@kit.edu (V. Metz), thorsten.schaefer@kit.edu (T. Schäfer).

subsurface installations of geothermal plants. Especially sulfate minerals with minor amounts of sulfides are encountered (Scheiber et al., 2014; Nitschke et al., 2014). The application of sulfate inhibitors efficiently reduces the amount of sulfate scales in the pipes. The geothermal site in Soultz Sous Forêts as an example, very successfully tested the application of a phosphonic acid based inhibitor (Scheiber et al., 2013; Scheiber et al., 2015). However, instead of sulfate dominated scales, ~3–5 mm thin brittle black scales are now forming at pipe walls in the surface installations, consisting of PbS, elemental Pb, As, Sb and minor oxide minerals. The deposition of sulfides and elemental lead in geothermal plants is a known phenomenon (Scheiber et al., 2013; Bressers et al., 2014). It is of concern due to the toxicity of Pb, As, and Sb, and due to the presence of  $^{210}\text{Pb}$  and its daughter nuclides in the scales, which are consequently classified as NORM (Naturally Occurring Radioactive Material).

A detailed mineralogical and chemical characterization of the deposited material is an obligatory prerequisite, to understand or predict the precipitation of these minerals out of the highly saline brine, and to develop tailored strategies to prevent their formation, e.g. with appropriate inhibitors. In this context this study reports detailed mineralogical and geochemical analyses based on various analytical methods, investigating six scale samples formed before and after the addition of sulfate scaling inhibitors to highly saline geothermal systems in the Upper Rhine Graben.

## 2. Sample origin

In the frame of this study, six scale samples (A–F) were investigated. They originate from three geothermal power plants in close proximity to each other. Samples A and B (in the following termed sulfate scalings) were collected before the application of a sulfate scaling inhibitor, the four samples C–F (in the following termed sulfide scalings) were deposited in the presence of an inhibitor. The geothermal sites in the Upper Rhine Graben and the composition of the produced geothermal brines are described in detail in (Sanjuan et al., 2016). Concerning the chemical composition of the produced brines, the geothermal plants in the Upper Rhine Graben are fairly similar. The average composition with respect to major and scale forming ions after (Sanjuan et al., 2016) is depicted in Fig. 1.

Samples A and B originate from two different geothermal sites. Both scales were deposited inside a heat exchanger. Samples were taken after regular cleaning work from canisters containing the removed scaling material. According to  $\gamma$  spectroscopic measurements the specific activity of sample A (about 1900 Bq/g) is dominated by  $^{226}\text{Ra}$ ,  $^{210}\text{Pb}$  and

$^{228}\text{Ra}$  (Köhler, 2013).

Samples C–F were collected at a third geothermal plant at four time intervals: sample C was taken first ( $t_0$ ), sample D at  $t_0 + 126$  days, sample E at  $t_0 + 253$  days, and sample F at  $t_0 + 420$  days. The samples were taken at one specific location in the water circuit from a pipe wall on the cold side (60 °C) of the heat exchanger. Two different ways of sampling and storing were chosen: 1. ambient conditions (C, D, part of E and F) and 2. under anoxic conditions (argon glove box) in order to minimize the oxidation of the samples for the purpose of assessing the oxidation state of As, Pb and Sb by means of X ray absorption near edge spectroscopy (pieces of E and F). Samples E and F were taken two and one day after a regular shut down of the geothermal plant, but with the pipes only emptied and opened just before sampling. They were placed in an argon bag immediately after sampling and rapidly transferred to an argon glove box, where they were stored until the XANES measurements.

## 3. Analytical methods

Scale samples are analyzed 1) after digestion by Inductively Coupled Plasma Mass Spectrometry (ICP MS, Element 2, Thermo Scientific), Ion Chromatography (IC, Metrohm 930 IC Flex) for Cl measurements according to DIN EN ISO 10304 1 (D 19), and Infrared Spectroscopy (IR) for TOC measurements according to DIN EN 1484, and 2) directly in solid state by X ray powder diffraction (XRPD, Bruker D8 Advance diffractometer), Scanning Electron Microscopy (SEM) and Energy Dispersive X ray fluorescence measurements (SEM EDX, FEI Quanta 650 FEG environmental SEM), X ray photoelectron spectroscopy (XPS, ULVAC PHI VersaProbe II), Isotope Ratio Mass Spectrometry (IRMS, IsoPrime, GV Instruments) coupled to an Elemental Analyzer (EA, HEKAtech), and Raman spectroscopy (BRUKER Senterra Raman microscope). Raman spectra were measured with depolarized laser beams at 532 nm (5 mW) and 785 nm (25 mW) excitation wavelengths, respectively. X ray absorption near edge spectroscopy (XANES) is employed to assess the oxidation state of As (As K edge, 11867 eV), Pb (Pb L<sub>III</sub> edge, 13035 eV) and Sb (Sb L<sub>III</sub> edge, 4132 eV) in the scale samples. XANES measurements are performed at the INE Beamline for actinide science at ANKA (Rothe et al., 2012). XRD patterns were semi quantitatively evaluated using the Bruker software DIFFRAC-EVA and TOPAS 4.2. For XANES data handling the IFEFFIT software package (Ravel and Newville, 2005) was used. All results reported in terms of percent refer to atom percent or mole fractions. Thermodynamic model calculations are performed using Phreeqc 3 (Parkhurst and Appelo, 2013) and the ThermoChimie

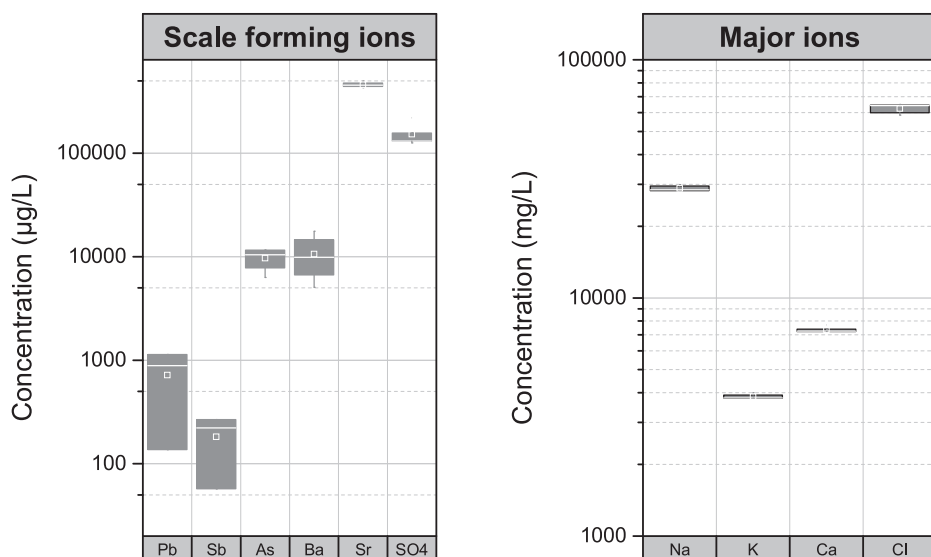


Fig. 1. Average chemical composition of the geothermal brines in the Upper Rhine Valley, with respect to scale forming and major ions (after Sanjuan et al., 2016).

**Table 1**  
Overview over the methods applied to investigate the various scaling samples.

	Digestion + chemical analysis	XRPD	SEM-EDX	XPS	EA-IRMS	Raman	XANES (As-K) (Pb-L <sub>III</sub> )	XANES (Sb-L <sub>III</sub> )
A		X	X	X		X		
B		X						
C	X	X	X	X	X		X	X
D	X	X	X		X		X	X
E <sup>a</sup>	X	X	X					X
F <sup>a</sup>		X	X					

<sup>a</sup> Samples stored under argon atmosphere directly after sampling (except the aliquot of sample E used for digestion and chemical analysis).

(SIT.dat) database (Giffaut et al., 2014). Elution tests after DIN EN 12457 4 are performed on bulk samples (C E), which were dried, ground, homogenized and stored under atmospheric conditions prior to the analysis. The eluent is water and the liquid to solid ratio 10 l/kg. The sulfur isotopy ( $\delta^{34}\text{S}$ ) was determined using dried bulk material (C, D). The certified reference materials IAEA S1, IAEA S3 and NBS127 have been used for calibration and quality assurance.

Not all methods could be employed on all samples. Table 1 gives an overview, which samples were analyzed by which methods. A complete discussion of all the analytical results would be beyond the scope of this work. In the following, those results will be highlighted, which are most important to understand the mineralogical and chemical characteristics of the samples, with a focus on the more recently investigated sulfide scalings (C F).

#### 4. Results

In the following section we present the results as obtained from the various applied methods for the two types of scaling samples.

##### 4.1. XRPD overview

A good overview of all the scale samples can be obtained by looking at the XRPD data presented in Fig. 2. As most of the samples contain a considerable amount of amorphous or nano crystalline material (up to 50%), conclusions about the quantitative composition are not based on the analysis of XRPD data. The difference between the sulfate dominated scalings A and B and the sulfide scalings C F is obvious. The majority of reflexes observed on samples A and B originates from a

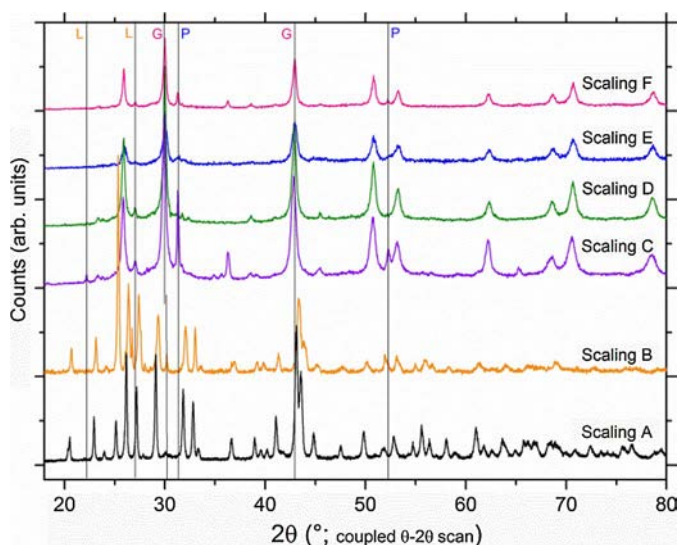


**Fig. 2.** XRPD data from scaling samples A-F. Thin vertical lines indicate main reflexes of some characteristic minerals: L-laurionite, G-galena, P-elemental lead. Scalings A and B are dominated by a barite type  $(\text{Ba,Sr})\text{SO}_4$  solid-solution. As reflex positions for this solid-solution vary with composition, no reflexes are marked for this mineral type.

barite type  $(\text{Ba,Sr})\text{SO}_4$  solid solution. A Rietveld model, in which the effect of composition on reflex position and reflex intensity are coupled via Vegard's law (Vegard, 1921), suggests a cation composition of 67%  $\text{BaSO}_4$  and 33%  $\text{SrSO}_4$  for sample A, and of 60%  $\text{BaSO}_4$  and 40%  $\text{SrSO}_4$  for sample B, respectively. Besides  $(\text{Ba,Sr})\text{SO}_4$ , XRPD indicates minor amounts of galena ( $\sim 1\%$  and  $2\%$ , respectively) in samples A and B.

For samples C F, galena is the main crystalline constituent, elemental lead shows sharp reflexes for samples C and F, and is present as low crystalline phase in sample E. Only traces of  $\text{Pb(0)}$  are identified in sample D. Laurionite  $(\text{PbCl(OH)})$ , a hydrothermal lead mineral, is clearly identified in samples C and D and plays only a minor role in samples E and F. It is interesting to note that, as indicated for the galena (002) reflex (around  $30^\circ$  in Fig. 2), galena shows a significantly increased dimension of the unit cell parameter in samples C F ( $a = 5.97 \text{ \AA}$  instead of  $5.93 \text{ \AA}$  (Noda et al., 1987)), whereas the galena unit cell parameter in samples A + B is close to the standard value. It is to date not clear, which type of impurity causes this enlargement of the unit cell. Likely candidates, as will be discussed below, are As or Sb. Traces of halite are present on some of the samples as a drying residue from the geothermal brine.

##### 4.2. Sulfate scalings: SEM EDX, Raman and XPS

Fig. 3 shows SEM images recorded from sample A. The left image shows the lamellar morphology of the barite type minerals. According to SEM EDX these have a cation composition of  $70.2 (\pm 0.7) \% \text{ Ba}$ ,  $26 (\pm 0.1) \% \text{ Sr}$  and  $3.8 (\pm 0.1) \% \text{ Ca}$ , which is in good agreement, with the XRPD analysis, especially regarding the fact that ternary solid solutions are difficult to include into an XRPD analysis. Based on  $\gamma$  spectroscopic measurements (Köhler, 2013) it is on the basis of crystal chemical considerations assumed that the barite type solid solution further incorporates trace amounts of natural Ra isotopes (mainly  $^{228}\text{Ra}$  and  $^{226}\text{Ra}$ ). The composition of the barite type minerals is corroborated by Raman spectroscopic measurements (cf. Supplementary information, Fig. S1). In Raman spectra, the position of the main sulfate band shifts linearly with the Ba/Sr ratio in the solid solution (Alía et al., 2000). It is at  $987.7 \text{ cm}^{-1}$  for pure barite and at  $1000.7 \text{ cm}^{-1}$  for pure celestite. The sulfate peak of the scaling sample is found at  $991.5 \text{ cm}^{-1}$  and corresponds to a Ba/Sr ratio of  $(71 \pm 4)/(29 \pm 4)$ .

The right image in Fig. 3 shows a mixed sulfide phase embedded in the lamellar barite type minerals. According to SEM EDX the sulfide phase has a cation composition of  $56.1 (\pm 1.3) \% \text{ Pb}$ ,  $26.0 (\pm 0.4) \% \text{ Sb}$ ,  $10.4 (\pm 1.3) \% \text{ As}$ , and  $7.5 (\pm 0.3) \% \text{ Cu}$ . A detailed analysis of the XPS sulfur (S 2p) spectrum (supplementary information, Fig. S2) revealed that the sulfate type minerals represent  $86 (\pm 9) \%$  of the sample, while the sulfide type minerals represent  $14 (\pm 2) \%$ . The amount of  $\text{S}^{2-}$  is approximately sufficient to satisfy the charge of Pb, As, Sb, and Cu, assuming that Pb and Cu are present as divalent cations, while As and Sb are present as trivalent cations. The Raman spectrum of the sulfide phase revealed similarities with meneghinite a hydrothermal  $\text{Pb Sb Cu sulfide (Pb}_{13}\text{CuSb}_7\text{S}_{24})$  (cf. Supplementary information Fig. S3). The minor amount of galena detected in sample A by means of XRPD was not identified in SEM images. For sample B no further information on potential X ray amorphous phases is available.

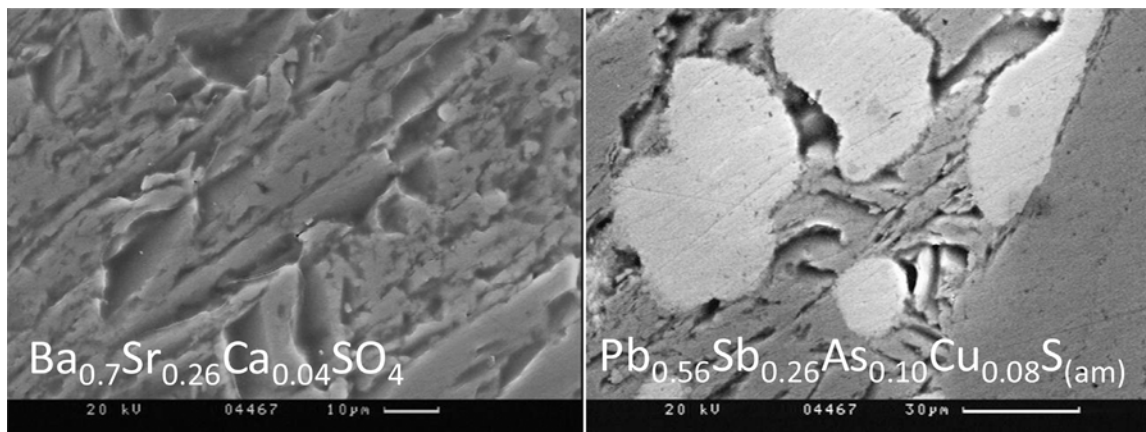


Fig. 3. SEM images recorded on scale A. The left image shows the lamellar morphology of the barite type solid solution. according to SEM-EDX it has a composition of  $Ba_{0.7}Sr_{0.26}Ca_{0.04}SO_4$ . The right image shows, embedded into the lamellar barite-type minerals, an amorphous mixed sulfide phase (Pb, Sb, As, Cu) $S_{(am)}$  with a cation composition: 56 % Pb, 26 % Sb, 10 % As, and 7 % Cu.

#### 4.3. Sulfide scalings: optical investigation

The optical images in Fig. 4 give an impression of the sulfide scalings (C F). Images in Fig. 4 are taken from sample E, immediately after sampling. The scaling material is very fragile and soft. The cross sectional view on the left in Fig. 4 shows the black dendrites growing from the pipe walls towards the interior. The bright spots at the surface of the scaling consist of elemental lead.

#### 4.4. Sulfide scalings: SEM EDX

Fig. 5 shows on the left hand side an overview SEM image of a cross section, recorded from an aliquot of sample E, which was embedded in epoxy resin, cut and polished. The solid material consists mostly of dendrites growing almost perpendicular from the pipe wall to the interior of the pipe. The branches of the dendrites grow independent of each other. Their diameter varies from  $\sim 2 \mu m$  up to  $30 \mu m$ , rarely up to  $100 \mu m$ , the length of the dendrites varies from a few  $\mu m$  up to  $2-3 mm$ . The right image shows a detailed image recorded on sample C. The asterisk marks a spot of an SEM EDX spot analysis on a dendrite. Dendrites consist of Pb, As, Sb, and S. In contrast to sample A, it is clear that the amount of sulfur in samples C F is not sufficient to characterize the dendrites as sulfide minerals (Table 2).

The dendrites are surrounded loosely by a very fine grained and porous material with a particle size of  $\sim 20 nm$  to  $1 \mu m$ . It consists of elemental Pb (bright fine grained particles in Fig. 6a, also visible in Figs. 5 and 6b (right)). Iron is present in all samples in variable

concentrations. Fe is identified as main element (besides oxygen) in very thin ( $\ll 0.1 \mu m$ ) flake like minerals (Fig. 6a and c). They are ubiquitous in the scalings. It is, however, difficult to determine their stoichiometry based on SEM EDX data. Iron minerals are not detectable by XRPD. Locally needle like Pb and Cl containing phases are identified, likely laurionite as also indicated by XRPD (Fig. 6d).

Fig. 7 shows a SEM EDX line scan over a selected region of sample F, which is dominated by dendrites. It nicely demonstrates the varying composition of the dendrites. Pb and S are quite evenly distributed along the scanline, and are present in a close to 1:1 ratio. A relation between this observation and the high amount of galena (PbS) identified by XRPD is likely. Particularly interesting is the anti correlated distribution of As and Sb. The dense central regions of the dendrites, which appear in light grey in the backscattered electron image in Fig. 7, are characterized by a close to 1:1 ratio of As and Sb. This may be an indication for stibarsen (SbAs). In between the dense dendrites, regions of lower electron density are encountered (darker grey in the backscattered electron image). These are characterized by an increasing As and decreasing Sb content up to a As/Sb ratio close to 3:1.

#### 4.5. Sulfide scalings: chemical analysis of the homogenized material

Table 2 presents the elemental composition of samples C, D, and E, as determined after digestion as described above. The sum of the elements listed corresponds approximately to 89.96% of the total solid. Focusing on the main elements Pb, S, Sb, and As, there is an excess of Pb over S, which may explain the presence of elemental lead besides

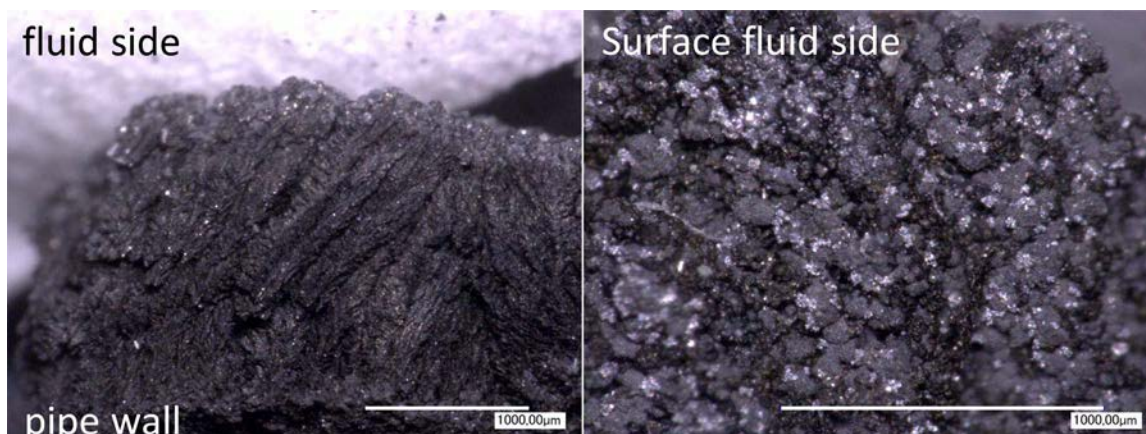


Fig. 4. Cross section (left) and surface (right) of the scaling sample E. Left) Black dendrites grow from the pipe wall towards the interior of the pipe. Right) Shiny spots on the surface consist of elemental lead.

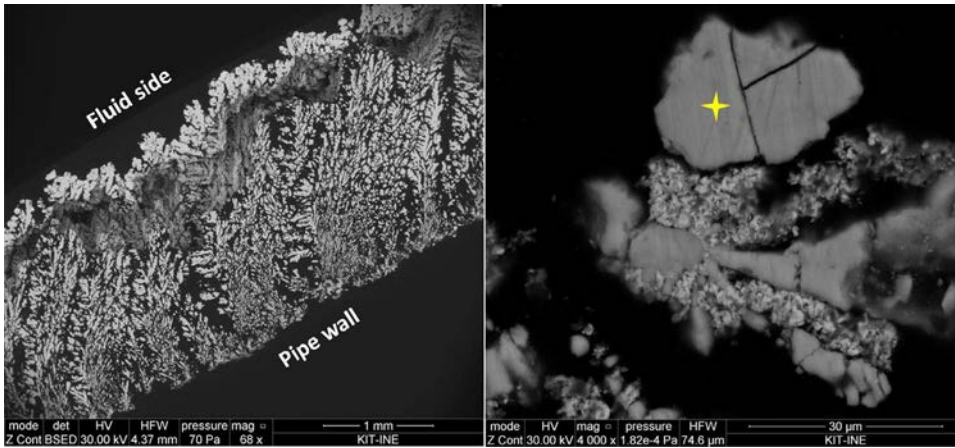


Fig. 5. SEM images as they are typical for the sulfide type scalings. Shown on the left is an overview cross section of an embedded aliquot of sample E. Dendrites light grey, resin black. The right image shows a detailed cross section of a dendrite recorded on sample C. The asterisk marks a spot of an EDX analysis (in atom-%): Pb 35, As 27, Sb 16, and S 22.

Table 2

Main elemental composition of the total solid of bulk samples C, D, and E in atom-%. The uncertainty related to the analytical results is approximately 10 %.<sup>a</sup>

Sample	Pb	S	Sb	As	Cu	Si	Ca	Fe	Na	K	Cl	TOC	Σ
C	31	19	13	12	0.2	1	2	1	5	0.5	6	2	92
D	23	19	15	13	0.1	13	1	1	4	0.3	4	2	96
E	23	16	13	14	0.2	2	1	12	3	0.4	3	2	89

<sup>a</sup> Relative to the reported value, not relative to the total amount.

galena. The Pb/S ratio is, however, not in quantitative agreement with XRPD and XANES. Sb and As are present in a close to 1:1 ratio indicating again the formation of stibarsen. Sample D contains a high amount of Si, the origin of which is unclear. Sample E contains a

considerable amount of iron, which matches with the increased presence of the iron rich flakes (Fig. 6a and c) in this sample. Na and Cl are drying residues of the brine solution.

#### 4.6. Sulfide scalings: sulfur isotopic analysis

To further elucidate the origin of the sulfide, sulfur isotope measurements were performed. Results in Table 3 are expressed as permil (‰) deviations from Canyon Diablo Troilite (CDT) using the conventional delta notation ( $\delta^{34}\text{S}_{\text{CDT}}$ ). Accuracy and reproducibility, determined by including the certified reference standards IAEA S1, IAEA S3 and NBS 127, are very high. The measured  $\delta^{34}\text{S}_{\text{CDT}}$  values in sample C and D are  $-18.45 (\pm 0.05) \text{‰}$  and  $-18.49 (\pm 0.01) \text{‰}$ , respectively. Because no sulfate minerals were detected in samples C and D, it

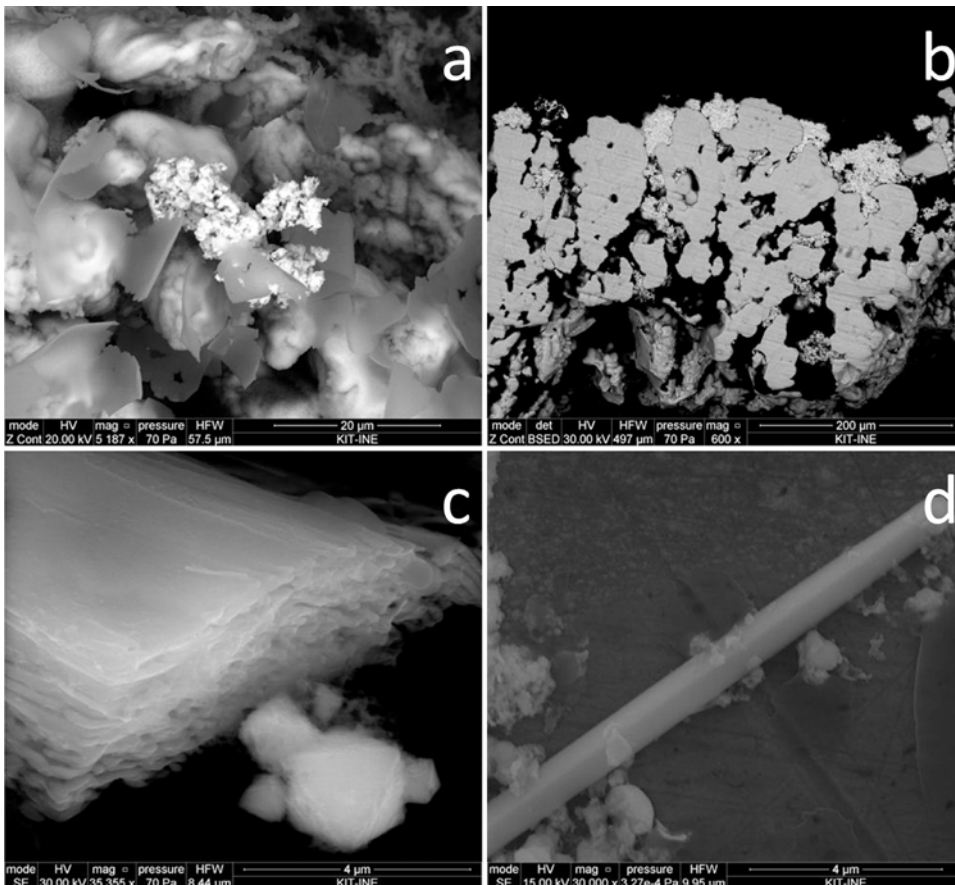


Fig. 6. A collection of detailed SEM images of sulfide scaling samples. Backscattered electron images: a) sample D, bright spots are elemental lead, flakes are Fe-rich platelets, b) morphology of the dendrites (grey) and surrounding porous elemental lead (light grey, sample E). Secondary electron images: c) flakes of Fe-rich platelets (sample D), d) idiomorphic laurionite needle (sample C).

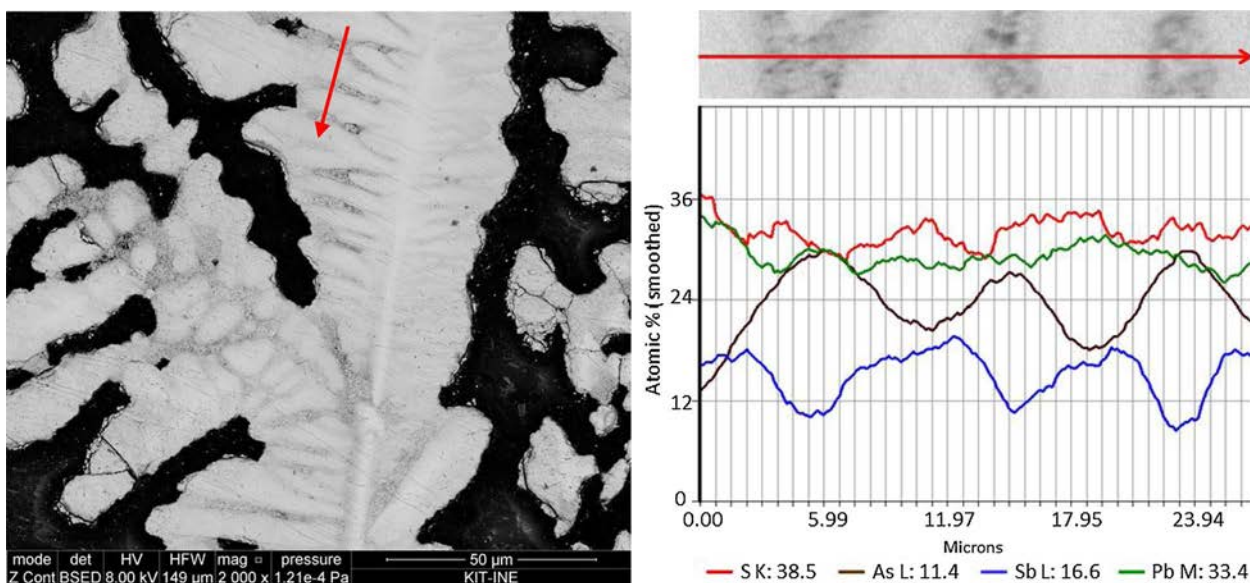


Fig. 7. Line scan over a selected region of a dendrite in scaling F. The left side shows a backscattered electron overview image of the dendrite. The region of the line scan is highlighted by a red arrow. On the right the Pb, S, As, and Sb distribution along the line scan is shown. The zoom above the scan data correlates the detailed position of the line scan with the measured data. (For interpretation of the references to colour in this figure legend, the reader is referred to the web version of this article.)

Table 3

Sulfur isotope ratios, standard deviations and number of measurements for dried bulk samples C and D, and certified references (in ‰).

Sample/reference	$\delta^{34}\text{S}_{\text{CDT}}$	Std	n
C	18.45	0.05	3
D	18.49	0.01	3
IAEA S1 (ref. value)	0.30 ( 0.30)	0.08	3
IAEA S3 (ref. value)	32.0 ( 32.0)	0.09	3
NBS 127 (ref. value)	21.16 (21.17)	0.09	6

can assumed that these isotopic signatures mainly represent the isotopic composition of sulfide minerals with PbS as major phase.

#### 4.7. Sulfide scalings: XANES analysis

The XRPD analysis, the overall chemical composition of the scale samples, and the stoichiometry of the phases identified by SEM EDX indicate that lead in the deposits is present as PbS and as elemental Pb (0). For the other main elements As and Sb it is largely unclear in which chemical form they are present, although, as already mentioned above, the lack of potential anions suggests that they are present in elemental form or as intermetallic mixtures (e.g. stibarsen). To analyze the redox state of Pb, As and Sb in the scaling samples in more detail XANES measurements were performed.

Pb L<sub>III</sub> edge XANES data measured on scaling C and D and two reference compounds Pb(0) and PbS are shown in Fig. 8. By means of linear combination fitting Pb in the samples is characterized as a mixture of PbS (90% – 95%) and Pb(0) (5% – 10%). This quantification is in line with XRPD data. It is, however, not in agreement with the overall element composition (Table 2), which likely suggests that the sulfur content is underestimated in the element analysis after digestion. Minor amounts of laurionite, identified by XRPD and SEM, seem not to significantly influence the XANES data.

As K edge XANES data are shown in Fig. 9. The fine structure of the absorption edges indicates that As(0), As(III), and As(V) are present in the scaling samples. A look at the 1<sup>st</sup> derivatives of the XANES data (Fig. 9, right) shows that As(V) likely plays only a minor role. It indicates that the samples are dominated by As(0) and show increasing oxidation to As(III) in the sequence  $D \ll C_1 \ll C_2$ . Some As(V) is certainly present as well, it is, however, overrepresented in the XANES

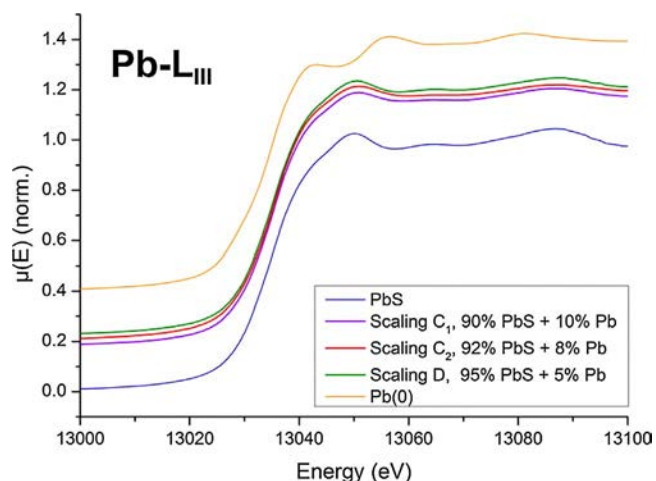
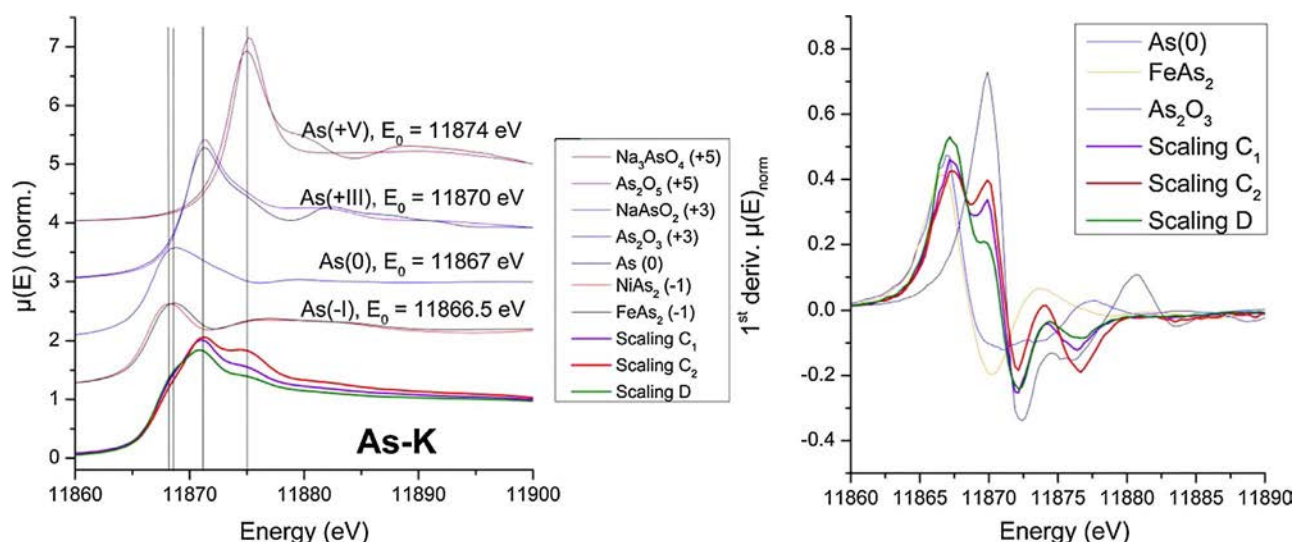


Fig. 8. Pb-L<sub>III</sub> edge XANES of samples C + D and two reference compounds PbS and Pb (0). Two separate aliquots of sample C, labelled C<sub>1</sub> and C<sub>2</sub> were investigated. Note that spectra are offset for clarity. The composition as quantified by linear combination fitting is detailed in the legend. (For interpretation of the references to colour in this figure legend, the reader is referred to the web version of this article.)

data, due to the very pronounced white line intensity related to this oxidation state. Scaling samples C and D were taken without special precautions against oxidation of the samples. Sample D was, however, dried within a few hours, while sample C was stored in a humid environment under atmospheric oxygen for six weeks prior to the measurements. Thus, it is expected that sample D is less oxidized compared to sample C. This means that the original scaling samples are likely dominated by As(0), and that As(III) and some As(V) develop upon storage at atmospheric conditions. This interpretation is also supported by corresponding results on Sb (Fig. 10).

Fig. 10 shows Sb L<sub>III</sub> edge XANES data of four scaling samples and the reference compounds Li<sub>3</sub>Sb, Sb(0), Sb<sub>2</sub>O<sub>5</sub>, Sb<sub>2</sub>S<sub>3</sub>, and Sb<sub>2</sub>O<sub>3</sub>. Again, samples C<sub>1</sub> and C<sub>2</sub> show a high degree of oxidation, while sample D is still in good agreement with Sb(0). Sample E, which was protected against oxidation directly after sampling in an inert gas atmosphere, agrees perfectly with the intermetallic reference compound Li<sub>3</sub>Sb.

Two details are particularly interesting: 1) instead of agreeing with



**Fig. 9.** As-K edge XANES of samples C + D and several reference compounds. Two separate aliquots of sample C, labelled C<sub>1</sub> and C<sub>2</sub> were investigated. Note that spectra are offset for clarity. On the left an overview over the XANES data is given. The approximate white-line positions of the various oxidation states are highlighted by vertical lines. To facilitate the interpretation in terms of absorption edge position, the 1<sup>st</sup> derivative of the normalized absorption edges is shown on the right. (For interpretation of the references to colour in this figure legend, the reader is referred to the web version of this article.)

the elemental Sb(0) reference, the unoxidized samples D and E agree almost perfectly with the intermetallic reference phase Li<sub>3</sub>Sb, 2) Sb(III) is not identified in the samples. Consequently, instead of a sequential oxidation as observed for arsenic: As(0) – As(III) – As(V), Sb seems, upon prolonged contact with air, to oxidize directly from elemental/intermetallic Sb to Sb(V) (cf. Fig. 10, right). XPS spectra measured on sample C did not provide important additional information (cf. supplementary information Fig. S4 for exemplary survey spectra).

#### 4.8. Sulfide scalings: elution tests

In order to evaluate the potential mobility of Pb, As, and Sb upon deposition in a landfill repository, elution tests were performed on samples C, D, and E (Table 4). The concentrations of Sb and As in the eluate exceed the German landfill regulations (Deponieverordnung, DepV) significantly.

## 5. Discussion

In this Discussion section the results of the various methods are summarized to arrive at scaling specific conclusions, and they are set in the context of previous work and for the sulfide scalings also related to thermodynamic considerations.

### 5.1. Sulfate scalings

Sample A + B, the sulfate scalings, show typical compositions as they have been previously described for scalings from geothermal sites in the Upper Rhine Graben (Nitschke et al., 2014; Scheiber et al., 2012; Mundhenk et al., 2013). The main phase of the scalings, which formed in the absence of a sulfate scale inhibitor, is a (Ba, Sr, Ca, Ra)SO<sub>4</sub> solid solution. While the Ba, Sr, Ca and sulfate composition of the barite type solid solution is determined by various analytical methods. The Ra content within the solid solution could not be determined directly. Besides the sulfate phase, minor amounts of galena (PbS) are observed. In sample A, additionally a mixed X ray amorphous (Pb, Sb, As, Cu)

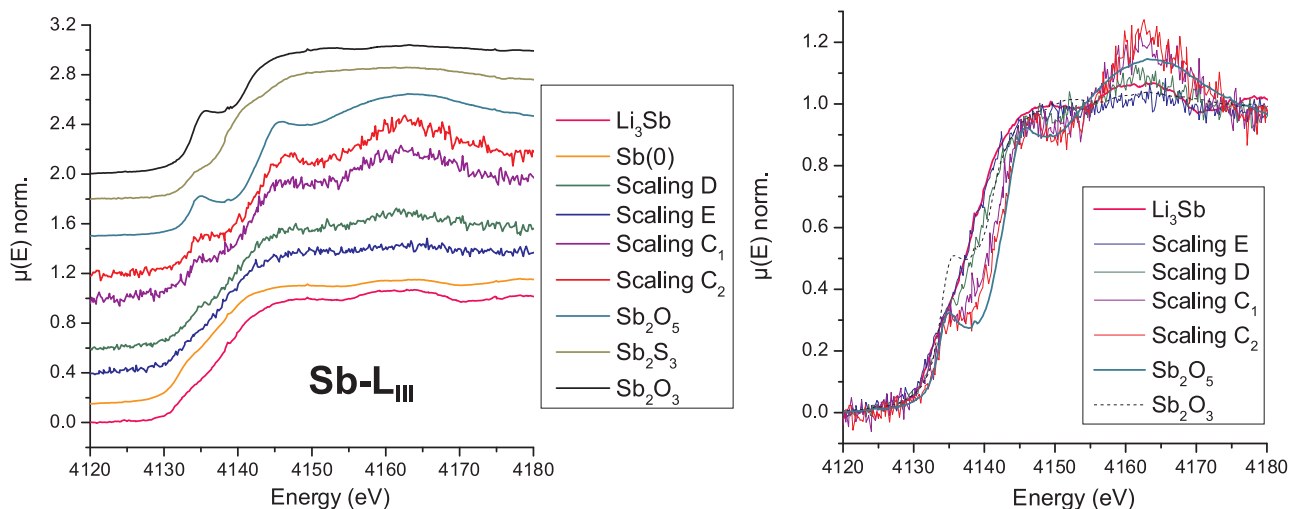


**Fig. 10.** Sb-L<sub>III</sub> edge XANES of samples C,D, and E and several reference compounds. Two separate aliquots of sample C, labelled C<sub>1</sub> and C<sub>2</sub> were investigated. On the left an overview over the XANES data is given. Note that spectra are offset for clarity. To facilitate the interpretation selected normalized absorption edges are directly overlaid on the right. (For interpretation of the references to colour in this figure legend, the reader is referred to the web version of this article.)

**Table 4**

Results of elution on homogenized samples C, D and E in eluate.

Sample	Pb (µg/L)	Sb (mg/L)	As (mg/L)	Cu (µg/L)	Zn (µg/L)	Cd (µg/L)	Ba (µg/L)	Conductivity (µS/cm)	pH
C	3840	28.8	199	14.4	81.8	20.3	147	6350	8.15
D	496	38.3	485	4.74	80.8	20.9	217	5250	7.57
E	4370	51.2	290	25.4	109	24	71.2	3440	7.66

S<sub>(am)</sub> phase was identified, the Raman spectra of which revealed some similarity with meneghinite. In contrast to samples C F, the stoichiometry of scale A suggests that As and Sb are present in a cationic form in sample A and the corresponding charge is compensated by sulfide (S<sup>2-</sup>) as anion. No carbonate phases were encountered. Because of the co precipitation of natural Ra isotopes with the sulfate solid solution, sulfate scalings are of radiological concern and need to be classified as NORM (Köhler, 2013; IAEA, 2003).

## 5.2. Sulfide scalings

The sulfide scalings, samples C F, collected after addition of sulfate inhibitors to the geothermal systems, contain mainly PbS, Pb(O), Sb(O), As(O) and to a lesser extent laurionite and oxidized species of Sb and As (Sb(V) and As(III) + As(V)). The occurrence of lead sulfide scalings is a well known matter of concern in oil and gas fields (Collins and Jordan, 2003; Jordan et al., 2000). Because of the application of the sulfate inhibitor PbS changes from a minor component to the main phase of the scaling material. Elemental lead deposition in geothermal plants has also been described before (Schmidt, 2000; Singh, 2015). Native lead and also laurionite as components of geothermal scalings were previously identified in Kamchatka Peninsula (Povarov et al., 2003), and in Northern Germany (Degering et al., 2011). Due to their <sup>210</sup>Pb content, the sulfide/elemental scalings still need to be classified as NORM. Ra deposition in sulfate phases is, however, largely avoided.

Concerning As and Sb speciation, our data indicate (especially for Sb) that oxidation of As and Sb occurs after the shutdown of the power plant, especially during subsequent storage of scaling samples at atmospheric conditions. As K XANES reveals that As speciation is dominated by low oxidation states. It is, however, hardly possible to distinguish between elemental As(0) and As(1) as it is e.g. present in lollingite (FeAs<sub>2</sub>). Particularly interesting are the Sb L<sub>III</sub> XANES spectra of the (more or less) unoxidized samples E and D. Their spectra show very good agreement with the reference phase Li<sub>3</sub>Sb, an intermetallic mix of Li<sup>+</sup> ions intercalated into Sb (Thackeray et al., 2003). Consequently, it is suggested that As and Sb are deposited during geothermal plant operation in a similar intermetallic state in a mixed phase. This finding solves any discrepancies with respect to the overall stoichiometry of the scalings, in which there is not enough sulfur to explain Pb, Sb, and As as cationic species bound in sulfide minerals (cf. Table 2 and Fig. 7).

Based on the XRPD data and the stoichiometry as indicated in Fig. 7 two possibilities to explain the composition of the dendrites are suggested. The first idea would be that Pb and S, which are more or less evenly distributed across the dendrites and in a close to 1:1 ratio, form galena, which is prominent in XRPD. Accordingly, As and Sb would most likely form an intermetallic (Sb, As) solid solution. It has been suggested before that the isostructural elemental Sb and As (space group: *R 3m*) form a solid solution series (Trzebiatowski and Bryjak, 1938). At temperatures ≥ 400 °C there seems to be complete mixing in this series. At lower temperatures especially the 1:1 mixture forms an ordered phase, stibarsen (SbAs) (Bayliss, 1991). It is intriguing to note that in a Rietveld model the uneven background of the XRPD data for samples C F can be well fit with a nano crystalline (crystal domain size ~2 nm) (Sb, As) solid solution, with unit cell parameters intermediate between that of As(O) and Sb(O) (space group *R 3m*, results not shown). Based on data in Fig. 7a possible composition of the dendrites

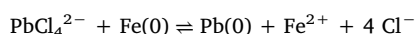
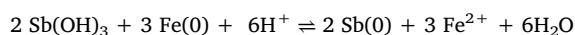
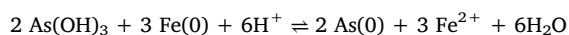
would be PbS + (Sb,As) in an approximate 3:2 ratio.

Based on the SEM images and EDX analyses one might as well suggest that Pb, Sb, As and S form one single mixed phase. A similar phase has to our knowledge not been described before. Such a phase should have a diffraction pattern similar to galena (cubic *Fm3m* or similar and length of the unit cell axis 5.97 Å instead of 5.93 Å). Searching the mindat.org database, eleven minerals are found that consist of Pb, Sb, As, and S. The majority of these (nine of eleven) have a stoichiometry in line with sulfide minerals, where Pb, As, and Sb are present as cations (x Pb(II) + y As(III) + z Sb(III) + (2x + 3y + 3z)/2 S(II)). Two minerals identified in an ore deposit in Finland (Borodav et al., 1983) have a stoichiometry in which Sb and As are more abundant than S, such that they cannot be simple sulfide minerals. The stoichiometry of these “mineral y” and “mineral z” are not similar to the dendrites in this study. Nevertheless, the previous identification of mixed phases containing Sb and As in excess over S, may confirm the possible formation of mixed phases as suggested here. However, no structural information about mineral y and z is available. According to data in Fig. 7, and assuming that dendrites are a single mixed phase, the composition of this phase could approximately be described as Pb<sub>3</sub>(Sb, As)<sub>2</sub>S<sub>3</sub>.

Regardless whether there is a mixture of galena and (Sb, As) or a single Pb<sub>3</sub>(Sb,As)<sub>2</sub>S<sub>3</sub> phase, there is presently no information available how these phases (except for galena) grow from aqueous solution, and what the related solubilities are.

A recent technology cluster (Bressers et al., 2014) investigated the electrochemical reactions between the metal parts of a geothermal installation and formation water. Beside the scalings, steel corrosion was their main concern. They suggest that the deposition of elemental lead is caused by electrochemical reactions in the system. Elemental arsenic was as well described as part of scalings in a heat exchanger system in the context of corrosion of carbon steel. Also here the authors consider electrochemical reactions as one of the reasons for As deposition (Julian et al., 2015). A scoping calculation on the oxidation/reduction of Fe, Pb, Sb, and As as a function of hydrogen partial pressure (Fig. 11, calculated for a 2 molal NaCl solution at 25 °C, pH 5.2 and 7.0) shows that at these conditions, which are comparable with the conditions at the geothermal power plant concerning pH and ionic strength (Sanjuan et al., 2016), Pb, As, and Sb are by far more noble (oxidize at higher pe) than iron.

This clearly points toward an electrochemical formation process for elemental Pb, As, and Sb, in which aqueous ions of Pb(II), As(III), or Sb(III) (according to SIT.dat mainly present as As(OH)<sub>3</sub>, Sb(OH)<sub>3</sub>, PbCl<sub>4</sub><sup>2-</sup> species) attach to the steel surface or to the surface of previously deposited Pb, As, or Sb and draw electrons from the steel. In exchange, Fe<sup>2+</sup> (or FeCl<sub>3</sub><sup>-</sup>) is released into solution. Corresponding reaction equations could be formulated as follows:



This would indicate that metal/metalloid scale formation is directly related to corrosion. On one hand such a corrosion mechanism could be easily minimized by applying a negative potential to the steel pipes, on the other hand, however, a negative potential applied on the steel could boost scale formation. A sacrificial anode, an isolating layer at the steel

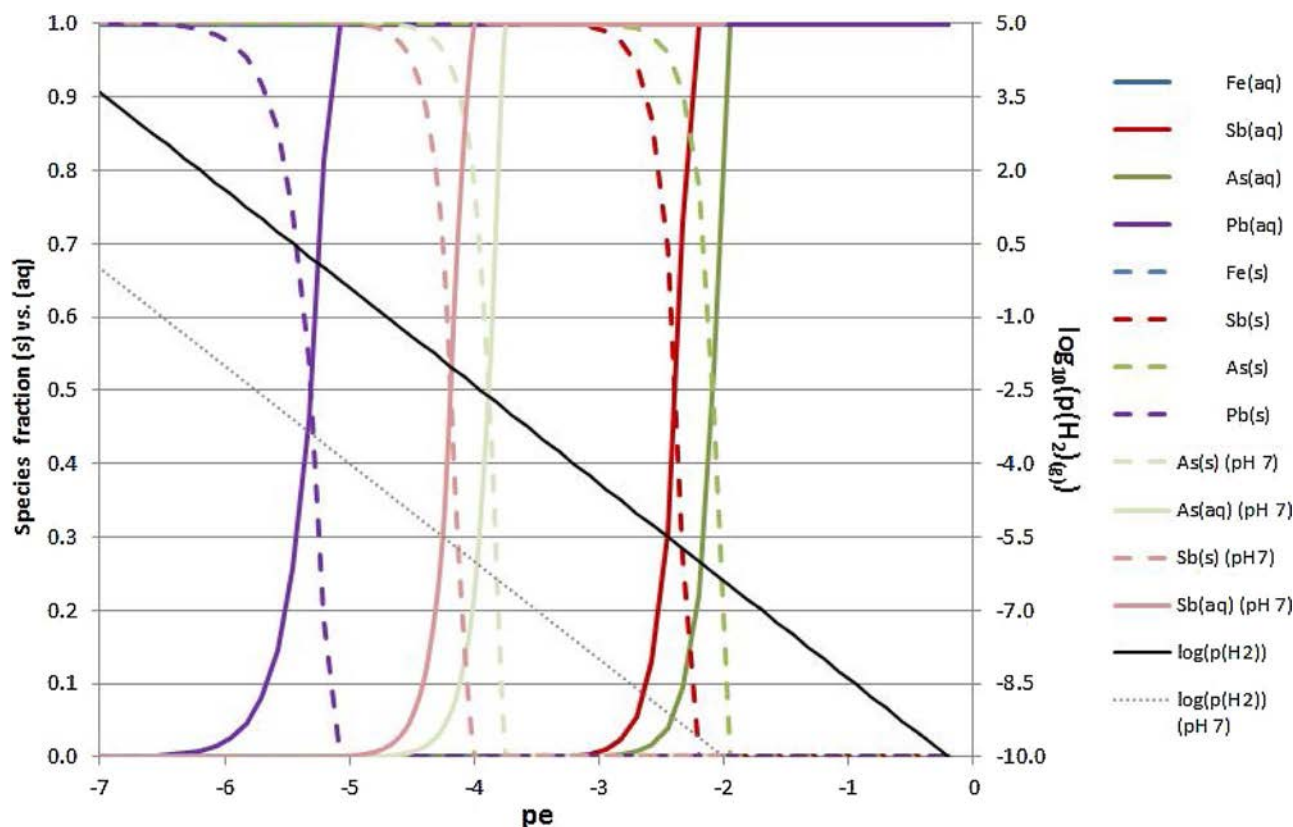


Fig. 11. Scoping calculation on the dissolution/precipitation of minor amounts (1 mmol/kg water) of elemental Fe, As, Sb, and Pb solids as a function of hydrogen partial pressure at pH 5.2 (and pH 7.0) at 25 °C in a 2 molal NaCl solution (Modeling with PhreeQC 3 (Parkhurst and Appelo, 2013) and the ThermoChimie (SIT.dat) database (Giffaut et al., 2014)). In the considered pH range, oxidation/reduction of Pb/Pb<sup>2+</sup> and Fe/Fe<sup>2+</sup> is independent of pH, while the pe where oxidation/reduction of As/As<sup>3+</sup> and Sb/Sb<sup>3+</sup> occurs, decreases with increasing pH. Note that the Fe/Fe<sup>2+</sup> transition is not reachable at reasonable hydrogen pressures in the considered pH range. It lies outside the plotted pe range at pe ≈ 10.5. (For interpretation of the references to colour in this figure legend, the reader is referred to the web version of this article.)

surface, or a type of inhibitor may be more promising to reduce corrosion as well as the formation of the elemental scalings. In any case, it may be expected that an efficient method to prevent corrosion (except applying a negative potential) would as well reduce the formation of elemental scalings, and vice versa. The complex interaction between the electrochemical reactions and the solubility of the deposited solid solutions at the relevant pressure, temperature, and ionic strength conditions certainly warrants further investigations.

Another important question regarding the redox state of the brine relates to the origin of sulfide in the brine and finally in the scalings. Important hints on the sulfide formation processes can be gained by comparing the  $\delta^{34}\text{S}$  values of sulfide scale minerals ( $-18.47\text{‰}$ ) with those of the dissolved sulfate ( $14.9\text{‰}$ ) (Sanjuan et al., 2016)) assuming aqueous sulfate as major S source. Sulfides that result from thermochemical sulfate reduction typically show a sulfur isotopic composition that is lighter than the original sulfate, by  $-3\text{‰}$  to  $-7\text{‰}$  in nature (Krouse, 1977; Machel et al., 1995; Orr, 1977) and up to  $-20\text{‰}$  in laboratory experiments (Machel et al., 1995). The S fractionation due to bacterial sulfate reduction is larger with  $-15\text{‰}$  to  $-30\text{‰}$  (Machel et al., 1995; Coleman et al., 1985). Consequently, the large fractionation of  $-33.4\text{‰}$  in our study strongly indicates microbial sulfate reduction and thus, biogenic origin of sulfide and related minerals (PbS). Electron donors that are necessary for microbial reductions are sufficiently provided by either the kerogen originating from the reservoir, the oil applied to the feed pump, or even the organic inhibitors, as manifested by the 2% TOC identified in samples C E (Table 2).

Scalings need to be removed from the pipes in order to maintain secure and efficient operation of the geothermal power plants. The corresponding solid waste material needs to be disposed of according to landfill regulations. Eluate tests (Table 4) show, however, a rather

strong elution of the elements As and Sb, which poses high demands for the disposal. The oxidation of As and Sb after prolonged storage at atmospheric conditions, as observed by XANES, indicates that the problem of As and Sb elution may even increase with time, because the resulting As(III), As(V), or Sb(V) minerals likely show considerably higher solubilities compared to the elemental phases. This problem constitutes a further challenge for geothermal power plant operation, which needs to be addressed.

## 6. Conclusion

In the geothermal power plants in the Upper Rhine Graben considered in this study, scale formation before the application of sulfate scale inhibitors was dominated by (Ba, Sr, Ca, (Ra))SO<sub>4</sub> solid solution scalings containing minor amounts of galena or mixed sulfide phases. The application of organic sulfate inhibitors suppresses the precipitation of sulfate minerals successfully. In the presence of inhibitors the precipitation of sulfides, metals and metalloids, predominantly PbS, Pb(O), As(O) and Sb(O) (likely as (Sb, As) or Pb<sub>3</sub>(Sb,As)<sub>2</sub>S<sub>3</sub>) solid solutions) is observed. Due to the high concentration of toxic heavy metals and metalloids in these scalings and due to their classification as NORM (because of the content of natural <sup>210</sup>Pb and its daughter nuclides) these sulfide/elemental scalings are of considerable concern. Thermodynamic/electrochemical considerations indicate that the deposition of elemental scalings may be directly related to corrosion. Isotope ratio measurements indicate a biogenic sulfide origin. Leaching tests demonstrate that further challenges arise with respect to the disposal of sulfide/elemental scalings.

## Competing interests

Detailed information about the name and the location of the geothermal plants, and the type and application protocol of the inhibitor are confidential. Thus we did not get the clearance to publish this information. Beyond that, the authors declare no competing interests.

## Acknowledgements

We acknowledge financial support by the German Federal Ministry for Economic Affairs and Energy (BMWi) through the collaborative project SUBITO (0325790A). The authors would like to thank our colleagues at KIT INE, in particular E. Soballa for sample preparation and for recording SEM images and SEM EDX data and J. Weißbach for assistance during XRPD and Raman spectroscopic analyses of sample A. Peter Adelmann (KIT IFP) and Silke Wolf (KIT AOC) are acknowledged for providing synthetic reference materials for the XANES study. KIT ANKA is acknowledged for the provision of beamtime. We thank Uta Czeslik for performing ICP MS measurements and Gesine Preuss (KIT AGW) for measuring S isotopes.

## References

- Alfá, J., Edwards, H., López-Andrés, S., González-Martin, P., Garcia-Navarro, F., Mansour, H., 2000. Ft-Raman study of three synthetic solid solutions formed by orthorhombic sulfates: celestite-barytes, barytes-anglesite and celestite-anglesite. *Spectrosc. Lett.* 33 (3), 323–336.
- Bayliss, P., 1991. Crystal chemistry and crystallography of some minerals in the tetradymite group. *Am. Miner.* 76 (1–2), 257–265.
- Borodaev, Y.S., Bortnikov, N., Mozgova, N., Ozerova, N., Oivanen, P., Yletyinen, V., 1983. Associations of Ore Minerals in the Deposits of the Seinäjoki District and the Discussion on the Ore Formation. *Bull. Geol. Soc. Finland* 55 (1), 3–23.
- Bressers, P., Wilschut, F., KKP, V., Floricultura, K., 2014. Lead deposition in geothermal installations. TNO internal report.
- Coleman, M., Berner, R., Durand, B., Meadows, P., Eglinton, G., 1985. Geochemistry of diagenetic non-silicate minerals kinetic considerations [and discussion]. *Phil. Trans. R. Soc. A: Math. Phys. Eng. Sci.* 315 (1531), 39–56.
- Collins, I., Jordan, M., 2003. Occurrence, prediction, and prevention of zinc sulfide scale within Gulf Coast and North Sea high-temperature and high-salinity fields. *SPE Prod. Facil.* 18 (03), 200–209.
- Degering, D., Köhler, M., Hielscher, M., 2011. Vorkommen und Verhalten natürlicher Radionuklide im Aquifer, im Fluid und in den Ablagerungen der Geothermieanlage Neustdt-Glewe. *Z. Geol. Wiss.* 39 (3/4), 275–290.
- Dezayes, C., Lerouge, C., Sanjuan, B., Ramboz, C., Brach, M., 2015. Toward a better understanding of the fluid circulation in the Rhine Graben for a better geothermal exploration of the deep basins. *World Geothermal Congress 2015*, vol. 2015.
- Giffaut, E., Grivé, M., Blanc, P., Vieillard, P., Colàs, E., Gailhanou, H., Gaboreau, S., Marty, N., Made, B., Duro, L., 2014. Andra thermodynamic database for performance assessment: ThermoChimie. *Appl. Geochem.* 49, 225–236.
- IAEA, 2003. Extent of environmental contamination by naturally occurring radioactive material (NORM) and technological options for mitigation. International Atomic Energy Agency, Vienna.
- Jordan, M.M., Sjursæther, K., Edgerton, M.C., Bruce, R., 2000. Inhibition of lead and zinc sulphide scale deposits formed during production from high temperature oil and condensate reservoirs. Society of Petroleum Engineers.
- Julian, R.H., Lichti, K.A.E.M.E., Mountain, B., 2015. Heavy metal scaling and corrosion in a geothermal heat exchanger. In: *World Geothermal Congress 2015*. Melbourne, Australia.
- Köhler, M., 2013. Untersuchungen Zum Umgang Mit Natürlicher Radioaktivität Bei Tiefer Geothermie: Abschlussbericht. BMU, Dresden, Hanover.
- Krouse, H., 1977. Sulfur isotope studies and their role in petroleum exploration. *J. Geochem. Explor.* 7, 189–211.
- Machel, H.G., Krouse, H.R., Sassen, R., 1995. Products and distinguishing criteria of bacterial and thermochemical sulfate reduction. *Appl. Geochem.* 10 (4), 373–389.
- Mundhenk, N., Huttenloch, P., Sanjuan, B., Kohl, T., Steger, H., Zorn, R., 2013. Corrosion and scaling as interrelated phenomena in an operating geothermal power plant. *Corros. Sci.* 70, 17–28.
- Nitschke, F., Scheiber, J., Kramar, U., Neumann, T., 2014. Formation of alternating layered Ba-Sr-sulfate and Pb-sulfide scaling in the geothermal plant of Soultz-sous-Forêts. *Neues Jahrbuch für Mineralogie-Abhandlungen: J. Miner. Geochem.* 191 (2), 145–156.
- Noda, Y., Masumoto, K., Ohba, S., Saito, Y., Toriumi, K., Iwata, Y., Shibuya, I., 1987. Temperature dependence of atomic thermal parameters of lead chalcogenides, PbS, PbSe and PbTe. *Acta Crystallogr. C* 43 (8), 1443–1445.
- Orr, W., 1977. Geologic and geochemical controls on the distribution of hydrogen sulfide in natural gas. *Adv. Organ. Geochem.* 50, 571–597.
- Parkhurst, D.L., Appelo, C., 2013. Description of input and examples for PHREEQC version 3—a computer program for speciation, batch-reaction, one-dimensional transport, and inverse geochemical calculations. *US Geological Survey Techniques and Methods, Book, vol. 6*. pp. 497.
- Povarov, O., Saakyan, V., Nikolski, A., Luzin, V., Tomarov, G., Sapozhnikov, M., 2003. Experience of creation and operation of geothermal power plants at Mutnovsky geothermal field, Kamchatka, Russia. In: *International Geothermal Conference*. Reykjavik, Iceland, Sept, 2003. pp. 14–17.
- Ravel, B., Newville, M., 2005. ATHENA, ARTEMIS, HEPHAESTUS. data analysis for X-ray absorption spectroscopy using IFEFFIT. *J. Synchrotr. Radiat.* 12, 537–541.
- Rothe, J., Butorin, S., Dardenne, K., Denecke, M.A., Kienzler, B., Löble, M., Metz, V., Seibert, A., Steppert, M., Vitova, T., Walther, C., Geckeis, H., 2012. The INE-beamline for actinide science at ANKA. *Rev. Sci. Instrum.* 83 (4).
- Sanjuan, B., Millot, R., Innocent, C., Dezayes, C., Scheiber, J., Brach, M., 2016. Major geochemical characteristics of geothermal brines from the Upper Rhine Graben granitic basement with constraints on temperature and circulation. *Chem. Geol.* 428, 27–47.
- Scheiber, J., Nitschke, F., Seibt, A., Genter, A., 2012. Geochemical and mineralogical monitoring of the geothermal power plant in Soultz-sous-Forêts (France). *Proceedings of the 37th Workshop on Geothermal Reservoir Engineering, 2012* 1033–1042.
- Scheiber, J., Seibt, A., Birner, J., Genter, A., Moeckes, W., 2013. Application of a scaling inhibitor system at the geothermal power plant in soultz-sous-Forêts: laboratory and on-Site studies. *Proceedings 2013*.
- Scheiber, J., Seibt, A., Birner, J., Cuenot, N., Genter, A., Moeckes, W., 2014. Barite scale control at the Soultz-sous-Forêts (France) EGS site. In: *Proceedings Thirty-Eighth Workshop on Geothermal Reservoir Engineering*. Stanford University, Stanford, California, 2014.
- Scheiber, J., Seibt, A., Birner, J., Genter, A., Cuenot, N., Moeckes, W., 2015. Scale inhibition at the Soultz-sous-Forêts (France) EGS site: laboratory and on-Site studies. In: *Proceed. World Geothermal Congress 2015*. Melbourne, Australia.
- Schmidt, A.P., 2000. Naturally occurring radioactive materials in the gas and oil industry: origin, transport and deposition of stable lead and <sup>210</sup>Pb from dutch gas reservoirs, vol. 195 Utrecht University.
- Singh, K.S.M., 2015. Review of the current state of the geothermal industry with a focus on the Netherlands.
- Thackeray, M.M., Vaughey, J.T., Johnson, C.S., Kropf, A.J., Benedek, R., Fransson, L.M.L., Edstrom, K., 2003. Structural considerations of intermetallic electrodes for lithium batteries. *J. Power Sour.* 113 (1), 124–130.
- Trzebiatowski, W., Bryjak, E., 1938. Röntgenanalyse des Systems Arsen–Antimon. *Zeitschrift für anorganische und allgemeine Chemie* 238 (2–3), 255–267.
- Vegard, L., 1921. Die Konstitution der Mischkristalle und die Rauffüllung der Atome. *Zeitschrift für Physik* 5 (1), 17–26.

## Repository KITopen

Dies ist ein Postprint/begutachtetes Manuskript.

Empfohlene Zitierung:

Haas-Nüesch, R.; Heberling, F.; Schild, D.; Rothe, J.; Dardenne, K.; Jähnichen, S.; Eiche, E.; Marquardt, C.; Metz, V.; Schäfer, T.

[Mineralogical characterization of scalings formed in geothermal sites in the Upper Rhine Graben before and after the application of sulfate inhibitors](#)

2018. Geothermics, 71

[doi: 10.554/IR/1000077988](#)

Zitierung der Originalveröffentlichung:

Haas-Nüesch, R.; Heberling, F.; Schild, D.; Rothe, J.; Dardenne, K.; Jähnichen, S.; Eiche, E.; Marquardt, C.; Metz, V.; Schäfer, T.

[Mineralogical characterization of scalings formed in geothermal sites in the Upper Rhine Graben before and after the application of sulfate inhibitors](#)

2018. Geothermics, 71, 264–273.

[doi:10.1016/j.geothermics.2017.10.006](#)